Probability uniformization and application to statistical palaeomagnetic field models and directional data

G Khokhlov, G Hulot

Geophysical Journal International

Geophys. J. Int. (2013) **193,** 110–121 doi: 10.1093/gji/ggs118

Probability uniformization and application to statistical palaeomagnetic field models and directional data

A. Khokhlov[1,2] and G. Hulot[2]

[1] *IEPT Russian Academy of Sciences,* 84/32, *Profsoyuznaya* 117997 *Moscow, Russia*

[2] *Equipe de Géomagnétisme, Institut de Physique du Globe de Paris, Sorbonne Paris Cité, Université Paris Diderot, INSU/CNRS* (UMR7154), 1, *rue Jussieu,* 75238, *Paris, France. E-mail: gh@ipgp.fr*

Accepted 2012 December 21. Received 2012 November 14; in original form 2012 April 29

SUMMARY

We introduce and apply the concept of 2-D probability uniformization to palaeomagnetic directional data. 2-D uniformization belongs to a very general class of probability transformations that map multivariate probability distributions into multivariate uniform distributions. Our goal is to produce joint tests of directional data sets assumed generated by a common statistical model, but with different sampling distributions. This situation is encountered when testing so-called Giant Gaussian Process (GGP) models of the Earth's magnetic field against palaeomagnetic directional data collected from different geographical sites, the predicted sampling distributions being site-dependent. To introduce the concept, we first consider 2-D Gaussian distributions in the plane $\mathbb{R}^2$, before turning to Angular Gaussian and more general 2-D distributions on the unit sphere S^2. We detail the approach when applied to the 2-D distributions expected for palaeomagnetic directional data, if these are to be consistent with a GGP model while affected by some Fisherian error. We finally provide some example applications to real palaeomagnetic data. In particular, we show how subtle inhomogeneities in the distribution of the data, such as the so-called right-handed effect in palaeomagnetism, can be detected. This effect, whether of geomagnetic origin or not, affects the Brunhes data in such a way that they cannot easily be reconciled with GGP models originally built with the help of these data. 2-D probability uniformization is a powerful tool which, we argue, could be used to build and test better GGP models of the mean palaeomagnetic field and palaeosecular variation. The software designed in the course of this study is available upon request from the authors. It can also be downloaded from http://geomag.ipgp.fr/download/PSVT.tgz.

Key words: Spatial analysis; Probability distributions; Magnetic field; Palaeomagnetic secular variation.

1 INTRODUCTION

It is a well-known fact that the main geomagnetic field exhibits a wide range of temporal variations and, at a particular time, depends continuously on spatial coordinates (see Hulot *et al.* 2010, for a recent review). Accurately reconstructing the spatiotemporal behaviour of this field requires that observations are regularly being made all over the globe. Such good spatiotemporal coverage can now be achieved thanks to satellites (e.g. Olsen *et al.* 2010), which nicely complement the ground-based network of observatories (e.g. Matzka *et al.* 2010). These, together with historical data, already provided enough data to reconstruct much of the Earth's magnetic field behaviour over the past few centuries (e.g. Jackson *et al.* 2000). Reconstructing the large scales of the field over the past few millennia is also possible, thanks to archeomagnetic data (e.g. Donadini *et al.* 2010), but going further back in time requires the use of palaeomagnetic data, that is, of palaeomagnetic field estimates reconstructed from rocks magnetized in the palaeofield. Unfortunately, age control of these rocks rarely ensures that data collected at various locations at the Earth's surface are synchronous enough (compared to the typical timescales involved in the field evolution, see, e.g. Lhuillier *et al.* 2011) that spatiotemporal reconstruction of the palaeomagnetic field remains possible. Important statistical properties of the palaeomagnetic field can nevertheless be recovered at the level of single sites (e.g. Love & Constable 2003), or more globally, by relying on general statistical representations of the palaeomagnetic field, such as the now widely used family of Giant Gaussian Process (GGP) models introduced by Constable & Parker (1988), and generalized by Hulot & Le Mouël (1994), Kono & Tanaka (1995), Tauxe & Kent (2004) and Hulot & Bouligand (2005).

These GGP models assume that during epochs of stable polarity, the main field behaved as a multidimensional stationary random Gaussian process with a short correlation time (a reasonable

assumption, see, e.g. Hongre *et al.* 1998; Bouligand *et al.* 2005). Under such circumstances, palaeofield estimates recovered from rock samples collected with a large enough time step at different locations can be considered as providing independent local (both in time and space) realizations of the underlying GGP.

Defining a GGP model then consists in providing a set of parameters defining the statistical behaviour of the magnetic vector at any geographical location: a set of Gauss coefficients $\{G_1^0, G_1^1, \ldots, G_l^m \ldots H_1^1, H_2^1, \ldots, H_l^m \ldots\}$ that defines the mean (or time-averaged) field about which the field fluctuates, and an (often simplified) covariance matrix $\mathrm{Cov}(\mathbf{k}, \mathbf{k}) = \left[\mathrm{cov}(k_i, k_j)\right]$, that defines the way the field fluctuates about this mean field (where the $\mathbf{k} = \{k_1, \ldots\}$ are the Gauss coefficients describing the time varying component of the field).

As explained in, for example, Constable & Parker (1988) or Khokhlov *et al.* (2001, 2006), such GGP models imply that vector samples $\mathbf{x} = (x_1, x_2, x_3)$ of the palaeofield at a given site at the Earth's surface will behave as if drawn from a 3-D Gaussian distribution defined by a mean vector $\mathbf{m} = (m_1, m_2, m_3)$ (in local cartesian coordinates) and a covariance matrix $\mathrm{Cov}(\mathbf{x}, \mathbf{x}) = \left[\mathrm{cov}(x_i, x_j)\right]$, the details of which depend on the site location, the mean field Gauss coefficients $\{G_l^m, H_l^m\}$ and the covariance matrix $\mathrm{Cov}(\mathbf{k}, \mathbf{k})$ of the GGP model (see, e.g. Khokhlov *et al.* 2001, 2006, for detailed formulae, which need not be made explicit here). If one introduces $\mathbf{\Lambda} = [\Lambda^{ij}]$, the inverse (hence, also symmetric) matrix of $\mathrm{Cov}(\mathbf{x}, \mathbf{x})$, this means that the field at the site location is expected to follow the 3-D-Gaussian probability density function (pdf)

$$\mathfrak{g}(\mathbf{x}) = \sqrt{\frac{\det \mathbf{\Lambda}}{(2\pi)^3}}\, \mathrm{e}^{-\frac{1}{2}(\mathbf{x}-\mathbf{m}, \mathbf{x}-\mathbf{m})_{\mathbf{\Lambda}}}, \tag{1}$$

where we make use of the $\mathbf{\Lambda}$-inner product $(\mathbf{x}, \mathbf{y})_{\mathbf{\Lambda}} = (\mathbf{\Lambda}\mathbf{x}, \mathbf{y}) = \sum_{i,j=1}^{3} \Lambda^{ij} x_i y_j$.

In principle, testing whether a GGP model is compatible with palaeomagnetic data simply consists in testing such pdfs against data at each site where data have been collected. However, these data are often sparse and only relatively few data can be tested against the corresponding distribution (1) for a given site (the parameters $\mathbf{m}$ and $\mathbf{\Lambda}$ of which depend on the site location, as already noted). In addition, these data are always measured and archived with some information about their errors, and this too needs to be taken into account.

When the data are vectorial, dealing with such issues is relatively straightforward. Vector errors can first be considered as independent Gaussian vectorial increments added to the error-free vector value. The corresponding 3-D-Gaussian error pdf can then be convolved with the 3-D-Gaussian pdf (1) to produce yet another 3-D-Gaussian pdf to be tested against the data from a given site. At such a single site, and for such a classical comparison, numerous statistical tests are available (e.g. Press *et al.* 2007). Simultaneously testing data from different sites (to test the regional or global compatibility of a GGP model against such data, assuming the data from different sites are independent) is then also possible. It just requires some preliminary data transformation to ensure that the local pdfs are reduced to a common standard isotropic 3-D-Gaussian distribution. This transformation is a linear coordinate change in the local (site) cartesian frame. Regional or global tests can then easily be performed by comparing the transformed data against the common 3-D-Gaussian pdf, again using standard tests. This possibility, however, is linked to the fact that all local data satisfy 3-D-Gaussian pdfs.

Unfortunately, most palaeomagnetic data are not 3-D-vectorial but directional-only. Such data no longer consist of $\mathbf{x} = (x_1, x_2, x_3)$ local cartesian coordinate values but of unit vectors $\mathbf{u} = \mathbf{x}/|\mathbf{x}|$, defined by inclination and declination $\{I, D\}$ values. Local tests against a GGP-model can no longer be done with the help of (1), but require the explicit form of the local pdf predicted by the GGP model in terms of the directional vector $\mathbf{u}$ on the unit sphere S^2. This pdf can be derived from (1) and takes the form of an Angular Gaussian distribution (Khokhlov *et al.* 2001, 2006). Errors in palaeomagnetic directional measurements are commonly treated as Fisherian (Fisher 1953; Fisher *et al.* 1987; Tauxe 2009). To test a given GGP model against a given directional data set with associated errors, one thus has to convolve a Fisher distribution with the local Angular Gaussian distribution (Khokhlov *et al.* 2006). Finally, simultaneously testing data from different sites also requires some preliminary data transformation. This is not as simple as in the case of vectorial data. In Khokhlov *et al.* (2001, 2006), we showed how a so-called 1-D uniformization could be used to transform all local Angular Gaussian directional distributions into a uniform distribution common to all sites. This procedure, however, converted the local 2-D Angular Gaussian distributions into just a 1-D distribution, ignoring the second dimension. This weakened the possibility of discriminating GGP models. In particular, it did not make it possible to statistically identify angular biases such as the well-known 'right-handed effect' first identified by Wilson (1970, 1971, 1972).

In this paper we therefore introduce a 2-D uniformization that generalizes and overcomes the limitations of the 1-D uniformization we previously used to test GGP models against data coming from different locations. This 2-D uniformization belongs to a very general family of multivariate probability transformations (e.g. Lévy 1937; Rosenblatt 1952; O'Reilly & Quesenberry 1973). However, our approach specifically takes the geometry of the problem into account. It is both very general and particularly well suited to test possible angular biases.

To illustrate the geometrical nature of this transformation, we introduce 2-D uniformization (Section 2) first for simple 2-D Gaussian distributions (Section 2.1), next for Angular Gaussian (and more general) distributions on the unit sphere (Section 2.2). We then apply this approach to the 2-D sampling distributions of palaeomagnetic directions generated by a GGP model while affected by some Fisherian error (Section 2.3). We finally illustrate the usefulness of 2-D uniformization using real palaeomagnetic data (Section 3), and conclude (Section 4).

2 2-D UNIFORMIZATION

2.1 2-D Gaussian distributions

We start from a simple geometrical construction in $\mathbb{R}^2$. Consider a unimodal random distribution that possesses rotational symmetry, for instance a centred Gaussian distribution with isotropic variances, that is, with pdf

$$\mathfrak{g}(\mathbf{x}) = \sqrt{\frac{\det \mathbf{\Lambda}}{(2\pi)^2}}\, \mathrm{e}^{-\frac{1}{2}(\mathbf{x},\mathbf{x})_{\mathbf{\Lambda}}} = \frac{\sqrt{\det \mathbf{\Lambda}}}{2\pi} \exp\left[-\frac{1}{2}\sum_{i,j=1}^{2} \Lambda^{ij} x_i x_j\right],$$
$$\mathbf{\Lambda} = \frac{1}{\sigma^2}\begin{pmatrix} 1 & 0 \\ 0 & 1 \end{pmatrix} \tag{2}$$

analogous to (1), except for the fact that we now deal with two dimensions, a zero mean and a much simplified axisymmetric $\mathbf{\Lambda}$ matrix.

We may define neighbourhoods of the most likely point (the origin here) in the following way: to a given $\hat{\mathbf{x}}$ we assign a neighbourhood

consisting of vectors $\mathbf{x}$ such that $\mathfrak{g}(\mathbf{x}) \geqslant \mathfrak{g}(\hat{\mathbf{x}})$. In the present case, this neighbourhood is nothing else than the disc of radius $|\hat{\mathbf{x}}|$. We may next compute the probability $\hat{t}$ that random data drawn from such a process appears in this neighbourhood:

$$\hat{t} = P\{\mathbf{x}|\mathfrak{g}(\mathbf{x}) \geqslant \mathfrak{g}(\hat{\mathbf{x}})\} = \iint_{\{\mathbf{x}|\mathfrak{g}(\mathbf{x}) \geqslant \mathfrak{g}(\hat{\mathbf{x}})\}} \mathfrak{g}(\mathbf{x})\, \mathrm{d}\mathbf{x}. \tag{3}$$

By construction, this probability takes all its values in [0, 1]. More generally, to any value $\mathbf{x}_i$ of a population $\{\mathbf{x}_i\}$ in $\mathbb{R}^2$ we may assign a value $t_i = P\{\mathbf{x}|\mathfrak{g}(\mathbf{x}) \geqslant \mathfrak{g}(\mathbf{x}_i)\}$ in [0, 1]. Then, again by construction, if the population $\{\mathbf{x}_i\}$ is statistically compatible with the pdf $\mathfrak{g}(\mathbf{x})$ in $\mathbb{R}^2$, the image population $\{t_i\}$ will be compatible with a uniform distribution in [0, 1]. This, in essence, is the principle of what we referred to as 1-D uniformization in Khokhlov *et al.* (2001, 2006). It makes it possible to test the radial distributions of the $\{\mathbf{x}_i\}$ population in $\mathbb{R}^2$. However, it does not allow the angular distribution of this population along the iso-probability lines $\mathfrak{g}(\mathbf{x}) = \mathfrak{g}(\hat{\mathbf{x}})$ to be tested. This is the limitation we now aim at overcoming, using a probability transformation akin to those initially introduced by Rosenblatt (1952), but specifically suited to the angular variable we are now interested in.

In the present example, since we consider a pdf (2) that possesses rotational symmetry, all iso-probability lines in $\mathbb{R}^2$ are circles (see Fig. 1). To assign a second, 'angular', statistical variable to $\hat{\mathbf{x}}$ (in addition to the 'radial' variable $\hat{t}$ just discussed), we first choose some arbitrary reference line Γ starting from the point of maximum probability (the origin, in the present instance) and crossing all iso-probability lines, for instance, here, a straight radial line (see Fig. 1). We next define A as the point of intersection of this reference line with the iso-probability line on which $\hat{\mathbf{x}}$ lies, and consider the arc length from A to $\hat{\mathbf{x}}$ along this iso-probability line (moving, say, anticlockwise). We finally introduce the ratio $\hat{s}$ of this arc length to the entire length of this (closed) iso-probability line. In the present instance, this geometrical construction simply amounts to dealing with trivial arc length measurements on the circle, the new variable $\hat{s}$ being equivalent to an angle normalized to take values in [0, 1]. However, it points at the general possibility of assigning in geometrical terms (just using the pdf and its iso-lines) a pair of independent statistical variables $(\hat{t}, \hat{s})$ to the initial $\hat{\mathbf{x}}$ variable, $(\hat{t}, \hat{s})$ taking values in [0, 1] × [0, 1], that is, in the unit square.

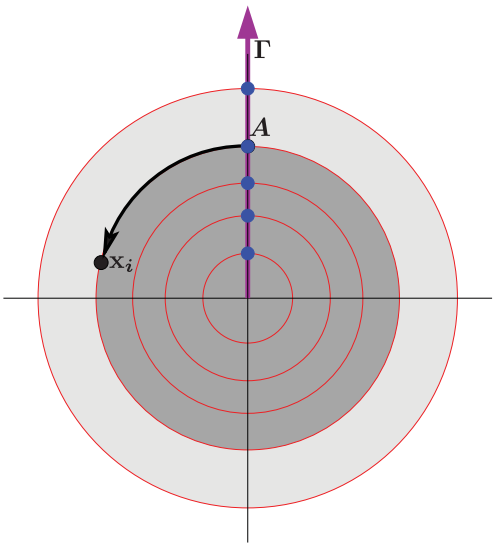

Figure 1. Uniformization of a 2-D Gaussian probability distribution function $\mathfrak{g}(\mathbf{x})$ in $\mathbb{R}^2$ (as defined by [2]). Shown are iso-probability lines (in the present case, circles), defining neighbourhoods of the origin, within which a randomly drawn point has a probability of (starting from the centermost) 10 per cent, 30 per cent, 50 per cent, 70 per cent and 90 per cent to lie. Also shown is a reference curve Γ (here a straight line going upwards) starting from the maximum at the centre of the distribution, intersecting at a point A the iso-probability line on which a typical realization $\mathbf{x}_i$ of the variable $\hat{\mathbf{x}}$ lies, to which we wish to assign realizations (t_i, s_i) of the uniformized variables $(\hat{t}, \hat{s})$. This is done by assigning to t_i the value of the probability associated with the neighbourhood limited by the iso-probability line on which $\mathbf{x}_i$ lies (the grey area corresponding here to $t_i = 0.70 = 70$ per cent), and assigning to s_i the ratio of the arc length joining A to $\mathbf{x}_i$ (counted anticlockwise, circular arrow) to the entire length of this (closed) iso-probability line.

Then, if we are given a random population $\{\mathbf{x}_i\}$ in $\mathbb{R}^2$ that is statistically compatible with the pdf $\mathfrak{g}(\mathbf{x})$, the corresponding (t_i, s_i) will be statistically compatible with a uniform distribution in the unit square [0, 1] × [0, 1]. However, now also, if the random population $\{\mathbf{x}_i\}$ is statistically incompatible with the pdf $\mathfrak{g}(\mathbf{x})$, then the (t_i, s_i) also will be statistically incompatible with a uniform distribution in the unit square. This example illustrates the main idea of 2-D uniformization: transforming of a 2-D statistical distribution into an equivalent uniform 2-D statistical distribution in the unit square.

Let us now consider a slightly more general unimodal case without rotational symmetry, for instance, a Gaussian distribution with anisotropic variances:

$$\mathfrak{g}(\mathbf{x}) = \sqrt{\frac{\det \mathbf{\Lambda}}{(2\pi)^2}}\, \mathrm{e}^{-\frac{1}{2}(\mathbf{x},\mathbf{x})_{\mathbf{\Lambda}}}, \quad \mathbf{\Lambda} = \begin{pmatrix} 1/\sigma_1^2 & 0 \\ 0 & 1/\sigma_2^2 \end{pmatrix}. \tag{4}$$

We may again construct a 'radial' variable $\hat{t}$ using (3), even though neighbourhoods are now elliptical. In contrast, the definition of the 'angular' variable $\hat{s}$ needs some improvement because the probability implied by (4) to have data in an angular sector is no more proportional to the corresponding angular measure, and must be corrected for the variations of the gradient of the pdf $\mathfrak{g}(\mathbf{x})$ along the iso-probability line $\mathfrak{g}(\mathbf{x}) = \mathfrak{g}(\hat{\mathbf{x}})$. To see this, consider the point $\hat{\mathbf{x}} + \mathrm{d}\mathbf{r}$, next to $\hat{\mathbf{x}}$, where $\mathrm{d}\mathbf{r}$ is an infinitesimal vector perpendicular to the iso-probability line $\mathfrak{g}(\mathbf{x}) = \mathfrak{g}(\hat{\mathbf{x}})$. Denote $\mathrm{d}r = |\mathrm{d}\mathbf{r}|$ and $\mathbf{n} = \mathbf{grad}\ \mathfrak{g}(\hat{\mathbf{x}})/|\mathbf{grad}\ \mathfrak{g}(\hat{\mathbf{x}})|$. Then $\mathrm{d}\mathbf{r} = \mathrm{d}r\mathbf{n}$. Also, $\hat{\mathbf{x}} + \mathrm{d}\mathbf{r}$ lies on the iso-probability line $\mathfrak{g}(\mathbf{x}) = \mathfrak{g}(\hat{\mathbf{x}} + \mathrm{d}\mathbf{r})$ and therefore $\mathrm{d}r = \mathrm{d}\mathfrak{g}/|\mathbf{grad}\ \mathfrak{g}(\hat{\mathbf{x}})|$, where $\mathrm{d}\mathfrak{g} = \mathfrak{g}(\hat{\mathbf{x}} + \mathrm{d}\mathbf{r}) - \mathfrak{g}(\hat{\mathbf{x}})$. Next define $\mathrm{d}\mathbf{l}$, an infinitesimal displacement starting from $\hat{\mathbf{x}}$ perpendicular to $\mathbf{n}$ and therefore along the iso-probability line $\mathfrak{g}(\mathbf{x}) = \mathfrak{g}(\hat{\mathbf{x}})$. Finally, consider the infinitesimal rectangle defined by the vector product of $\mathrm{d}\mathbf{r}$ with $\mathrm{d}\mathbf{l}$, of surface $\mathrm{d}r\,\mathrm{d}l$. The probability of finding a point $\mathbf{x}$ in this rectangle, based on the pdf $\mathfrak{g}(\mathbf{x})$, is then $\mathfrak{g}(\hat{\mathbf{x}})\mathrm{d}r\ \mathrm{d}l = \mathfrak{g}(\hat{\mathbf{x}})\mathrm{d}\mathfrak{g}|\mathbf{grad}\ \mathfrak{g}(\hat{\mathbf{x}})|^{-1}\mathrm{d}l$.

Now, just as in the previous case, we may choose some arbitrary reference line starting from the point of maximum probability (again the origin, in the present instance) and crossing all iso-probability lines (note that this can again be a straight radial line). We may also again define A as the point of intersection of this reference line with the iso-probability line $\mathfrak{g}(\mathbf{x}) = \mathfrak{g}(\hat{\mathbf{x}})$ which we will denote $L(\hat{\mathbf{x}})$, and consider the arc $L(A, \hat{\mathbf{x}})$ from A to $\hat{\mathbf{x}}$ along this iso-probability line (moving again anticlockwise). Finally, we may sum (integrate) the probabilities of finding a point $\mathbf{x}$ in the surface included between this arc and the adjacent infinitesimally close arc along the iso-probability line $\mathfrak{g}(\mathbf{x}) = \mathfrak{g}(\hat{\mathbf{x}} + \mathrm{d}\mathbf{r})$. This leads to $\int_{L(A,\hat{\mathbf{x}})} \mathfrak{g}(\mathbf{x})\mathrm{d}\mathfrak{g}|\mathbf{grad}\ \mathfrak{g}(\mathbf{x})|^{-1}\mathrm{d}l$. Normalizing this quantity by its maximum value, corresponding to the circular integration along the (closed) iso-probability line $L(\hat{\mathbf{x}})$, and taking into account the fact

that both $\mathfrak{g}(\mathbf{x})(=\mathfrak{g}(\hat{\mathbf{x}}))$ and $\mathrm{d}\mathfrak{g}$ take constant values in the integrals, we may finally introduce the quantity:

$$\hat{s} = \frac{\int_{L(A,\hat{\mathbf{x}})} |\mathbf{grad}\ \mathfrak{g}(\mathbf{x})|^{-1}\mathrm{d}l}{\int_{L(\hat{\mathbf{x}})} |\mathbf{grad}\ \mathfrak{g}(\mathbf{x})|^{-1}\mathrm{d}l}, \tag{5}$$

which takes values in [0, 1] and generalizes the definition we previously introduced for $\hat{s}$ in the axisymmetric case. For this previous axisymmetric case, indeed, $|\mathbf{grad}\ \mathfrak{g}(\mathbf{x})|$ takes a constant value in both integrals, and $\hat{s}$ reduces to $\hat{s} = \int_{L(A,\hat{\mathbf{x}})} \mathrm{d}l / \int_{L(\hat{\mathbf{x}})} \mathrm{d}l$.

Then by construction, and as in this previous case, if we are given a random population $\{\mathbf{x}_i\}$ in $\mathbb{R}^2$ that is statistically compatible (respectively incompatible) with the pdf $\mathfrak{g}(\mathbf{x})$ (now given by [4]), the corresponding $\{(t_i, s_i)\}$ (computed by setting $\hat{\mathbf{x}} = \mathbf{x}_i$ in [3] and [5]) will be statistically compatible (respectively incompatible) with a uniform distribution in the unit square $[0, 1] \times [0, 1]$. 2-D uniformization of the original 2-D statistical distribution into a uniform 2-D statistical distribution in the unit square is thus again achieved.

It is important to note that, whereas a linear coordinate transform can be used to reduce a general Gaussian distribution to a standard one (for instance, to reduce the pdf given by [4] to that given by [2]), the above geometric construction now directly relies on integrations of the pdf to be tested (for the implementation, see the Appendix). This characteristic of the 2-D uniformization approach makes it readily applicable to the stable polarity palaeomagnetic case we will later focus on, where data no longer consist of 2-D-vectors $\mathbf{x} \in \mathbb{R}^2$ but of unit directional vectors $\mathbf{u} \in S^2 \subset \mathbb{R}^3$.

2.2 Angular Gaussian distributions and 2-D distributions on the unit sphere

We now consider the case of Angular Gaussian distributions. These correspond to distributions of directional vectors $\mathbf{u} = \mathbf{x}/|\mathbf{x}|$ on the unit sphere S^2 when the 3-D vectors $\mathbf{x}$ in $\mathbb{R}^3$ follow a 3-D-Gaussian distribution of the most general form given by (1), with mean vector $\mathbf{m}$ and covariance matrix $\mathrm{Cov}(\mathbf{x}, \mathbf{x}) = \mathbf{\Lambda}^{-1}$. If we introduce the spherical coordinates $(\mathbf{u}, \rho)$ of the vector $\mathbf{x}$ (where $\rho = |\mathbf{x}|$), then the pdf associated with the direction $\mathbf{u}$ on S^2 is given by:

$$\mathfrak{s}(\mathbf{u}) = \int_0^\infty \mathfrak{g}(\rho\mathbf{u})\,\mathrm{d}\rho, \tag{6}$$

where $\mathfrak{g}(\rho\mathbf{u}) = \mathfrak{g}(\mathbf{x})$ is defined by (1). Eq. (6) defines the Angular Gaussian distribution associated with the 3-D-Gaussian distribution (1). Note that this Angular Gaussian distribution thus results from integration over all lengths ρ of the 3-D-Gaussian distribution and is different from the Bingham distribution (Bingham 1964; Love 2007), which results from intersecting the 3-D-Gaussian distribution by the unit sphere $S^2 \subset \mathbb{R}^3$. As shown by Khokhlov *et al.* (2001, 2006) (see also Bingham 1983, for series expansions in the case of an Angular Gaussian distribution corresponding to an isotropic 3-D-Gaussian distribution)), eq. (6) can be integrated into the explicit formula:

$$\mathfrak{s}(\mathbf{u}) = e^{-\frac{1}{2}m^2} \cdot \frac{\sqrt{\det \mathbf{\Lambda}}}{4\pi |\mathbf{u}|_{\mathbf{\Lambda}}^3} \left[z\sqrt{\frac{2}{\pi}} + e^{\frac{1}{2}z^2}(1+z^2)\left[1+\mathrm{Erf}\left(\frac{z}{\sqrt{2}}\right)\right]\right], \tag{7}$$

where (making use of the $\mathbf{\Lambda}$-norm $|\mathbf{x}|_{\mathbf{\Lambda}} = \sqrt{(\mathbf{x}, \mathbf{x})_{\mathbf{\Lambda}}}$)

$$z = \frac{(\mathbf{m}, \mathbf{u})_{\mathbf{\Lambda}}}{|\mathbf{u}|_{\mathbf{\Lambda}}}, \qquad m = |\mathbf{m}|_{\mathbf{\Lambda}}, \tag{8}$$

correspond to, respectively, the $\mathbf{\Lambda}$-projection of $\mathbf{m}$ on the direction $\mathbf{u}$ and the $\mathbf{\Lambda}$-norm of $\mathbf{m}$. Note that since $\mathbf{\Lambda}$ is positive, $-m \le z \le m$.

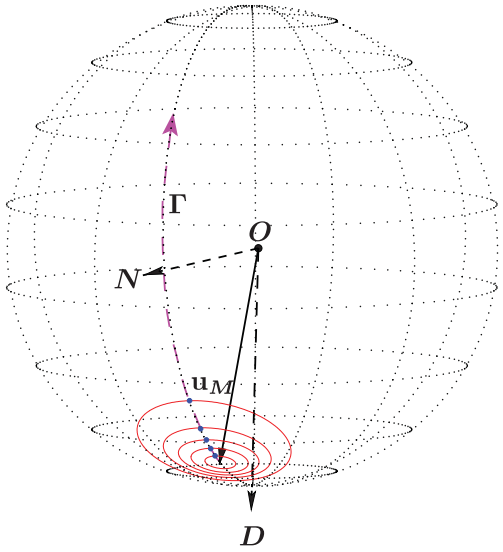

Figure 2. Example of an Angular Gaussian probability distribution function $\mathfrak{s}(\mathbf{u})$ on the unit sphere S^2 (as defined by [7]). Here the QC GGP model (see definition in Section 3) has been used for a site at 50°N, 7°E. O is the centre of the unit sphere; D and N respectively point Down and North at the local site. Shown are iso-probability lines defining neighbourhoods of the most likely direction $\mathbf{u}_M$, within which a randomly drawn direction has a probability of, respectively, 10 per cent, 30 per cent, 50 per cent, 70 per cent and 90 per cent to lie. The reference curve Γ needed for 2-D uniformization (see text) has been defined as the curve starting from $\mathbf{u}_M$, moving up in the Down/North plane.

Such distributions can be quite complex. However, if $|\mathbf{m}|$ is large enough compared to the square roots of the entries of the matrix $\mathrm{Cov}(\mathbf{x}, \mathbf{x})$, then the corresponding Angular Gaussian distribution will be unimodal, such as the one shown in Fig. 2. This will be the case when considering Angular Gaussian distributions predicted by the most plausible GGP models at the Earth's surface (see Khokhlov *et al.* 2001, 2006).

Consider now the direction $\mathbf{u}_M \in S^2$ for which $\mathfrak{s}(\mathbf{u})$ takes it global maximum value $\mathfrak{s}_{\mathrm{Max}}$. Then there exists a value $\mathfrak{s}_0 < \mathfrak{s}_{\mathrm{Max}}$ such that any iso-probability line $\mathfrak{s}^{-1}(y)$, $y \in (\mathfrak{s}_0, \mathfrak{s}_{\mathrm{Max}})$ is a closed one-component curve. Furthermore, if we happen to know that $\mathfrak{s}(\mathbf{u})$ is unimodal, then the only other extremum point of $\mathfrak{s}(\mathbf{u})$ is where it takes its minimum value $\mathfrak{s}_{\mathrm{Min}}$, in which case we may set $\mathfrak{s}_0 = \mathfrak{s}_{\mathrm{Min}}$ and all iso-probability lines on S^2 are known to be closed one-component curves, analogous to the circles and ellipses in $\mathbb{R}^2$ encountered in the previous section. Under such circumstances, we may again choose a smooth curve Γ starting from $\mathbf{u}_M$ and transverse to any iso-probability curve (see Fig. 2). Then, to any direction $\hat{\mathbf{u}}$ on S^2, we may again assign a pair of two variables $(\hat{t}, \hat{s})$ such that:

$$\hat{t} = \iint_{\{\mathbf{u}|\mathfrak{s}(\mathbf{u}) \ge \mathfrak{s}(\hat{\mathbf{u}})\}} \mathfrak{s}(\mathbf{u})\,\mathrm{d}U, \qquad \hat{s} = \frac{\int_{L(A,\hat{\mathbf{u}})} |\mathbf{grad}\ \mathfrak{s}(\mathbf{u})|^{-1}\mathrm{d}l}{\int_{L(\hat{\mathbf{u}})} |\mathbf{grad}\ \mathfrak{s}(\mathbf{u})|^{-1}\mathrm{d}l}, \tag{9}$$

where $L(\hat{\mathbf{u}})$ is the entire (closed) iso-probability line $\mathfrak{s}(\mathbf{u}) = \mathfrak{s}(\hat{\mathbf{u}})$ on which $\hat{\mathbf{u}}$ lies, and $L(A, \hat{\mathbf{u}})$ is the portion of this iso-probability line between its intersection A with the curve Γ and $\hat{\mathbf{u}}$ (some common orientation being chosen for all iso-probability lines). Indeed, since all values $\mathfrak{s}(\hat{\mathbf{u}})$ are regular (except $\mathfrak{s}_{\mathrm{Max}}$ and $\mathfrak{s}_{\mathrm{Min}}$, both of which correspond to isolated critical points), $|\mathbf{grad}\ \mathfrak{s}(\mathbf{u})|$ is never zero in the integrals defining $\hat{s}$, and $\hat{s}$ is thus always defined. It can then readily be checked that the reasonings that led to (3) and (5) can be repeated here to show that if we are now being given a random population $\{\mathbf{u}_i\}$ in S^2 that is statistically compatible (respectively

incompatible) with the pdf $\mathfrak{s}(\mathbf{u})$ (given by [7]), the corresponding $\{(t_i, s_i)\}$ (computed by setting $\hat{\mathbf{u}} = \mathbf{u}_i$ in [9]) will be statistically compatible (respectively incompatible) with a uniform distribution in the unit square $[0, 1] \times [0, 1]$. 2-D uniformization of the original 2-D statistical distribution in S^2 is thus again achieved.

The above reasoning can be applied (together with the uniformization formulae [9]) to any 2-D statistical distribution in S^2, provided it is unimodal and smooth enough. In fact, it can also be applied to multimodal distributions, albeit in a slightly different way. One can again take advantage of the fact that a vicinity of the absolute maximum $\mathbf{u}_M$ of the pdf can always be defined within which any iso-probability line $\mathfrak{s}^{-1}(y)$ is a closed one-component curve. Within this vicinity, a smooth curve Γ (starting from $\mathbf{u}_M$ and transverse to any iso-probability curve) can again be found and formulae (9) applied (with appropriate renormalization of $\hat{t}$ to the maximum value it may take in this vicinity, which is when $\hat{\mathbf{u}}$ is lying on the iso-probability line bounding the vicinity), to achieve 2-D uniformization of the original 2-D statistical distribution within this vicinity. More generally, one may then also define similar vicinities for all secondary maxima of the pdf in S^2, apply the same procedure to each vicinity, and finally repeat this also for minima (in which case the definition of $\hat{t}$ needs another slight change to sum iso-probabilities smaller, rather than larger, than the iso-probability corresponding to $\hat{\mathbf{u}}$), to achieve what may then be referred to as piecewise 2-D uniformization of the original 2-D statistical distribution.

2.3 2-D uniformization of palaeomagnetic directional distributions

We now turn to the more specific case of palaeomagnetic directional distributions. Consider a given site at the Earth's surface where directional measurements are available ($\{\mathbf{u}_1, \ldots \mathbf{u}_i, \ldots\}$ distributed on the unit sphere S^2), that we wish to use to test a given GGP model. As already noted, the directional distribution predicted at such a site by such a GGP model for error-free data is an Angular Gaussian probability distribution of the form $\mathfrak{s}(\mathbf{u})$ as defined by (7), the parameters of which depend on both the GGP model parameters (mean Gauss coefficients $\{G_1^0, G_1^1, \ldots, G_l^m \ldots H_1^1, H_2^1, \ldots, H_l^m \ldots\}$, and covariance matrix $\mathrm{Cov}(\mathbf{k}, \mathbf{k}) = [\mathrm{cov}(k_i, k_j)]$), and the site location. If the data were perfect, 2-D uniformization of this data set would thus simply consist in applying the procedure described in Section 2.2 for Angular Gaussian distributions.

However, the data are not perfect, and errors must be taken into account. Furthermore, some data may have larger errors than others. Finally, we may want to consider data coming from different sites. It thus is important that each datum is considered individually. Assuming directional errors to be Fisherian, as is usually considered appropriate, this means that for each datum $\mathbf{u}_i$ characterized by a Fisherian error with concentration parameter K_i, this datum must be compared to the pdf considering all possibilities of drawing a value $\mathbf{w}$ from $\mathfrak{s}_i(\mathbf{w})$ defined by (7) at the site where these data were collected, and next drawing a value $\mathbf{u}$ from the Fisher distribution $\mathfrak{k}_{K_i}(\mathbf{u}, \mathbf{w})$ centred on $\mathbf{w}$ and defined by

$$\mathfrak{k}_K(\mathbf{u}, \mathbf{w}) = \frac{K}{2\pi\ (\mathrm{e}^K - \mathrm{e}^{-K})} \mathrm{e}^{K\mathbf{u}\cdot\mathbf{w}}. \tag{10}$$

As discussed in Khokhlov *et al.* (2006), this amounts to compare $\mathbf{u}_i$ to the pdf $\mathfrak{p}_i(\mathbf{u})$ defined by

$$\mathfrak{p}_i(\mathbf{u}) = \iint_{S^2} \mathfrak{s}_i(\mathbf{w}) \mathfrak{k}_{K_i}(\mathbf{u}, \mathbf{w})\, \mathrm{d}\mathbf{w}. \tag{11}$$

It is important to note that K in (10) is the concentration parameter defining the error affecting the directional datum, and not the one defining the dispersion of the samples used to estimate this datum. For practical applications, this concentration parameter can be inferred from the α_{95} parameter, usually provided with the data, using formulae such as (A4) in Khokhlov *et al.* (2006). This is the formula we use when referring to α_{95} values in our software and in the examples provided below.

Even though there may be only one datum $\mathbf{u}_i$ to compare to each pdf $\mathfrak{p}_i(\mathbf{u})$ at a time, 2-D uniformization can now be used to collect, without any loss of information, the statistical information brought by the entire data set $\{\mathbf{u}_1, \ldots \mathbf{u}_i, \ldots\}$ for comparison against the background GGP statistical model. For each directional datum $\mathbf{u}_i$ in S^2, one just needs to compute the uniformized pair of values (t_i, s_i), using the same rules as established in Section 2.2 (recall [9]), but corresponding to the relevant pdf $\mathfrak{p}_i(\mathbf{u})$:

$$t_i = \iint_{\{\mathbf{u}|\mathfrak{p}_i(\mathbf{u}) \geqslant \mathfrak{p}_i(\mathbf{u}_i)\}} \mathfrak{p}_i(\mathbf{u})\, \mathrm{d}U, \quad s_i = \frac{\int_{L_i(A_i, \mathbf{u}_i)} |\mathbf{grad}\ \mathfrak{p}_i(\mathbf{u})|^{-1} \mathrm{d}l}{\int_{L_i(\mathbf{u}_i)} |\mathbf{grad}\ \mathfrak{p}_i(\mathbf{u})|^{-1} \mathrm{d}l}, \tag{12}$$

where $L_i(\mathbf{u}_i)$ is the entire (closed) iso-probability line $\mathfrak{p}_i(\mathbf{u}) = \mathfrak{p}_i(\mathbf{u}_i)$ on which $\mathbf{u}_i$ lies, and $L_i(A_i, \mathbf{u}_i)$ is the portion of this iso-probability line between its intersection A_i with a reference curve Γ_i and $\mathbf{u}_i$. In principle the reference curve Γ_i can be chosen independently for each datum $\mathbf{u}_i$. However, it is important that some simple common rule be used for all data to keep a useful meaning to the new quantity s_i. In what follows, we will thus systematically define Γ_i in the same way as the Γ curve shown in Fig. 2, that is, as the curve starting from the maximum of $\mathfrak{p}_i(\mathbf{u})$, moving up in the Down/North plane. Similarly, s_i will be computed using (12), with $L_i(A_i, \mathbf{u}_i)$ counted clockwise when looking at the distribution on the unit sphere from the outside (as is the case in Fig. 2), so that small values of s_i correspond to $\mathbf{u}_i$ pointing slightly westwards of the Down/North plane, and values close to unit correspond to $\mathbf{u}_i$ pointing slightly eastwards of this plane.

Then, testing if the sequence of directional measurements $\{\mathbf{u}_1, \mathbf{u}_2, \ldots\}$ is a random population that is statistically compatible with the GGP model (assumed as a background process), given the known individual Fisherian errors $\mathfrak{k}_{K_i}$, is equivalent to testing that the population $\{(t_1, s_1), (t_2, s_2), \ldots\}$ is statistically compatible with a uniform distribution in the unit square $[0, 1] \times [0, 1]$. 2-D uniformization of the palaeomagnetic directional data distribution has been achieved.

3 APPLICATIONS TO REAL PALAEOMAGNETIC DATA

To illustrate the usefulness of 2-D uniformization, we now apply it to real palaeomagnetic data. The database Q94 we will use is that of Quidelleur *et al.* (1994), to ease comparisons with the studies of Khokhlov *et al.* (2001, 2006).

We start with Brunhes normal polarity data from sites 17 (data selected from Böhnel *et al.* 1987) and 18 (selected from Böhnel *et al.* 1982), which we will test against the normal polarity GGP model C1 of Quidelleur & Courtillot (1996) (their preferred model, empirically built to fit the Q94 database, to which we will refer as the QC model and which we will use up to degree 7, as in Khokhlov *et al.* 2006, where the model parameters are fully specified). The reason for this choice is that the combined data from these two sites, which share the same location of 50°N, 7°E, have been shown to be marginally compatible with this model when only 1-D uniformization is applied (Khokhlov *et al.* 2006). Yet, these data plot in a way

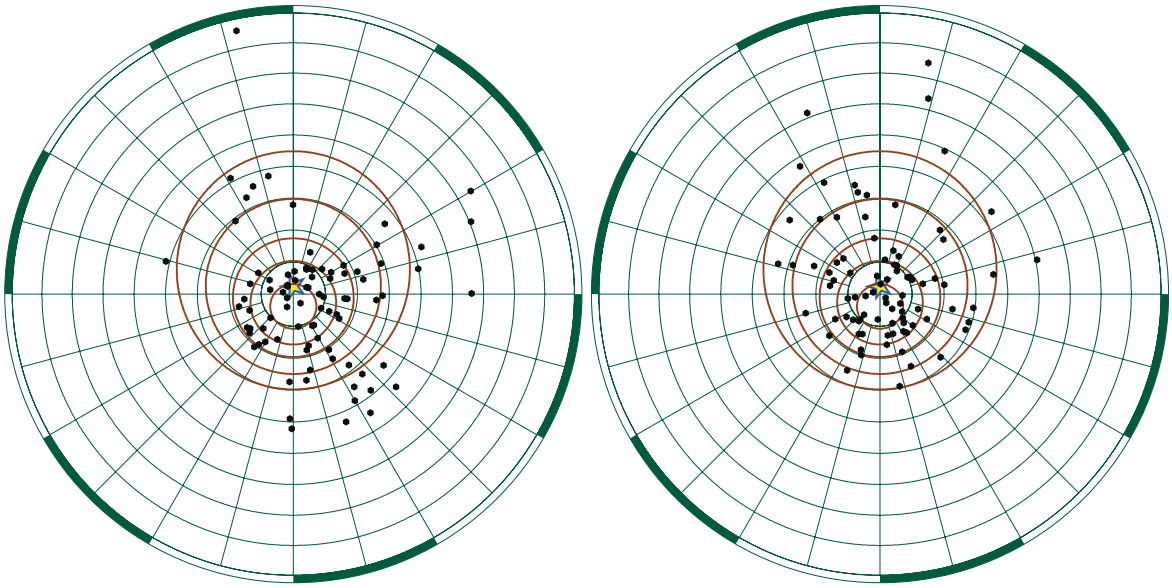

(a) (b)

Figure 3. Combined data from sites 17 and 18 of the Q94 database, at 50°N, 7°E, Lambert-projected, the centre point (pointing downwards through the page) corresponding to the direction produced by a pure axial dipole at this location; North towards the top of the page, East towards the right. Angular distances with respect to the centre of the plot are shown every 5° (green circles). Isovalues of a common $\mathfrak{p}_i(\mathbf{u})$ pdf (computed from (11), using the predicted pdf for the QC model at the site location and a common Fisher distribution, assuming an error of $\alpha_{95} = 3.72^\circ$ for all data) are shown as red ellipses. Those correspond to the bounds within which, respectively, 10 per cent, 30 per cent, 50 per cent, 70 per cent, 90 per cent of the data points should plot. (a) Real data; (b) equal amount (88) of synthetic data (see text for details).

that strongly suggests that they do not at all comply with the QC model.

To see this, we use the same plotting convention as in fig. 3 of Khokhlov *et al.* (2006, see our Fig. 3). As noted earlier, each datum $\mathbf{u}_i$ having a different error estimate, must be tested against its own $\mathfrak{p}_i(\mathbf{u})$ pdf. However, and as in Khokhlov *et al.* (2006), to be able to plot all the data against a single $\mathfrak{p}_i(\mathbf{u})$ pdf (and only for the specific purpose of showing such a figure), we plot the $\mathfrak{p}_i(\mathbf{u})$ pdf computed from (11), using the pdf predicted by the QC model at the site location, and the Fisher distribution corresponding to the mean $\alpha_{95} = 3.72^\circ$ of the errors of all the data plotted (Fig. 3a). A second similar plot with synthetic data is also shown for reference (Fig. 3b). These data are generated one at a time, with $\mathfrak{p}_i(\mathbf{u})$ adjusted at each draw to exactly match the assumed error of one true datum for each datum generated. This second plot illustrates how the same number of synthetic data intrinsically compatible with the QC model, and affected by the same individual errors as the true data, generally plot.

Fig. 3 clearly suggests that compared to the synthetic data plot, too many data are to be found eastwards and southwards of the expected distribution in the real data plot, even though both plots display roughly the same proportion of data within each iso-probability lines. As we shall now see, 2-D uniformization of the data makes it possible to confirm this.

After 2-D uniformization into $\{(t_1, s_1), (t_2, s_2), \dots\}$ (each data now being assigned its individual error), the data $\{\mathbf{u}_1, \mathbf{u}_2, \dots\}$ that were plotted in Fig. 3 may first be plotted in the unit square $[0, 1] \times [0, 1]$, where they are now expected to be uniformly distributed. Fig. 4 clearly shows that this is not the case for the real data plot, which displays voids and a tight cluster around $t = 1$ and $s = 0.5$ (corresponding to the south-eastward excess of data in Fig. 3a).

To ease the interpretation of these voids and clusters, we may next recognize that whereas t_i can be interpreted as a renormalized distance of $\mathbf{u}_i$ to the most likely direction $\mathbf{u}_M$ on the unit sphere, s_i reflects a renormalized angular measure of the distance of $\mathbf{u}_i$ from the Down/North plane along the iso-probability line $\mathfrak{p}_i(\mathbf{u}_i)$. This suggests that we also plot the uniformized data on a disc of unit radius, using $(t_i, 2\pi s_i)$ as polar coordinates. The result of this is shown in Fig. 5. Note that the data plotted in this way are not expected to be uniformly distributed in the disc (the pdf being inversely proportional to the radial distance for such a representation, as one can easily check). However, it is expected to be equally distributed in all radial directions. Fig. 5 makes it clear that this is not the case and that the real data are unlikely to be compatible with the QC model, even when data errors are taken into account, because too many data plot in a single sector. This prompts us to turn to more quantitative tests. Indeed, plenty of tests are available to test the compatibility of a 2-D data set against a uniform distribution in the unit square.

We first repeat a test already carried out in Khokhlov *et al.* (2006), where 1-D uniformization was already used. In this previous study, the $\{t_i\}$ as defined by (12), were indeed already considered, and their expected uniform distribution in the unit segment [0, 1] tested. This was achieved by using two classical tools, the Kolmogorov–Smirnov test (KS-test) and the Anderson–Darling test (AD-test). These two tests rely on the fact that, if a given data set $\{x_i\}$, $i = 1, \dots N$ is compatible with a uniform distribution over [0, 1], its empirical cumulative distribution function (cdf) $F_N(x)$ should fluctuate within known limits about the theoretical cdf value $F(x) = x$. The tested hypothesis should then be rejected if the empirical cdf $F_N(x)$ departs too much from x. The KS-test and AD-test differ in the measure chosen to assess how distant $F_N(x)$ is from x over [0, 1]:

(i) the KS-test uses the maximum value M_N of $|F_N(x) - x|$ over [0, 1], and is therefore most sensitive to departures of the $\{x_i\}$ from a uniform distribution towards the middle of the segment [0, 1];

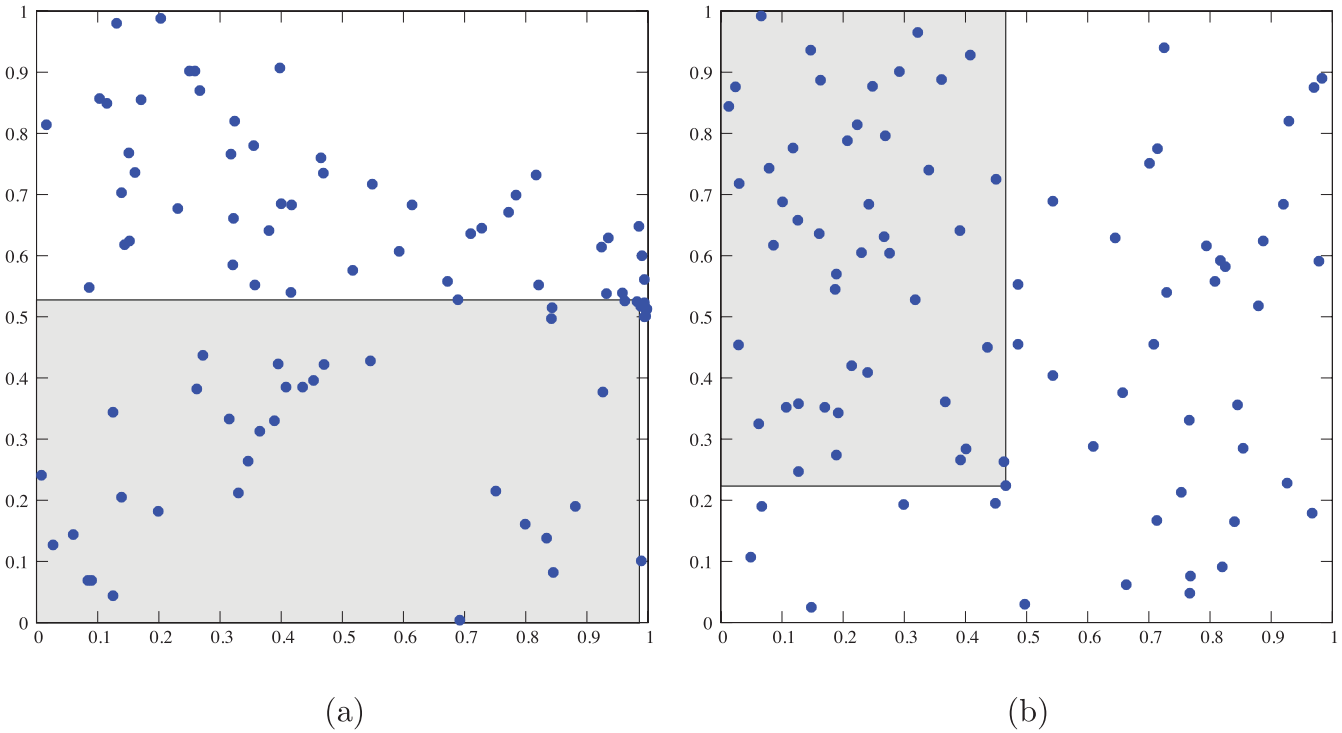

Figure 4. Same data as in Fig. 3, but plotted in t (abscissa) and s (ordinate) coordinates in the unit square $[0, 1] \times [0, 1]$ after 2-D uniformization. (a) Real data; (b) synthetic data. Highlighted in grey are the quadrants identified by the FF test (see text for details).

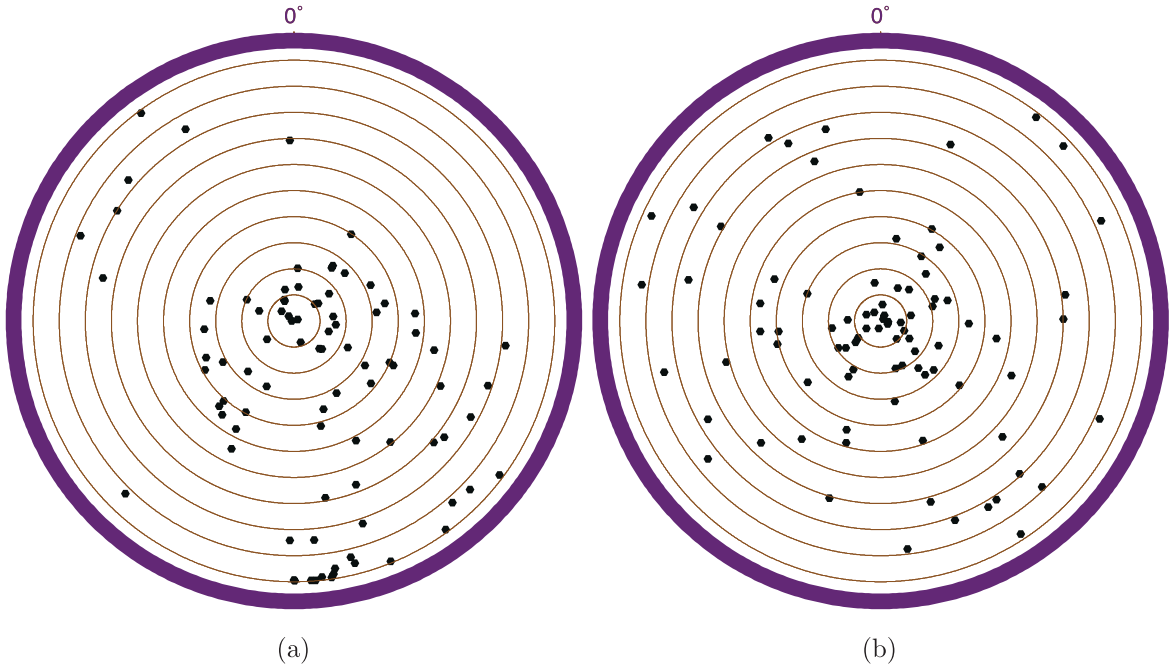

Figure 5. Same data as in Figs 3 and 4, but plotted in polar $(t, 2\pi s)$ coordinates in a disc of unit radius. Origin for the angular coordinate $2\pi s$ is taken at the top of the disc, corresponding to North in Fig. 3, and isovalues for t are plotted with 0.1 steps, to allow comparison with Fig. 3 and ease identification of matching data points. This figure may be seen as an unfolded version of Fig. 3, taking into account the topology imposed by the $\mathfrak{p}_i(\mathbf{u})$ pdfs. (a) Real data; (b) synthetic data.

(ii) the AD-test uses the integral quantity $I_N = N \int_0^1 (F_N(x) - x)^2 [x(1-x)]^{-1} dx$. Because of the weight $[x(1-x)]^{-1}$, it is much more sensitive to the behaviour of $\{x_i\}$ at both extremes of the segment [0, 1].

To apply these tests, one just needs to compute the values of M_N and I_N from the data set $\{x_i\}, i = 1, \ldots N$ to be tested, and infer (from known software, e.g. Marsaglia & Marsaglia 2004; Press *et al.* 2007) the probabilities $P(M_N)$ and $P(I_N)$ for the null hypothesis to have

possibly produced such large, or even larger, values for, respectively, M_N and I_N. Then, if $P(M_N)$ or $P(I_N)$ is found to take a value very close to 0 (typically 0.05 or less), the tested hypothesis can be rejected at the corresponding level of confidence (here 95 per cent).

Applying these tests to the 1-D uniformized data $\{t_i\}$ from the combined sites 17 and 18 ($N = 88$ data), leads to $M_N = 0.118$ and $I_N = 3.25$ with probabilities $P(M_N) = 0.16$ and $P(I_N) = 0.02$. (Note that these values differ slightly from the values $M_N = 0.16$ and $I_N = 3.20$ with probabilities $P(M_N) = 0.17$ and $P(I_N) = 0.02$ provided by Khokhlov *et al.* (2006) for the same test, because we now use a different numerical scheme to compute the convolution involved in (11), based on a computation on the spherical grid, using a fast SHT transform spherical convolution, see the Appendix). These results confirm the conclusion of Khokhlov *et al.* (2006) that if only the 1-D uniformized data $\{t_i\}$ are investigated, the data shown in Fig. 3 are only very marginally consistent with the QC GGP model. The most stringent AD-test indeed rejects the compatibility of these data with the QC model at the 98 per cent level of confidence. This reflects the slight trend seen in both Figs 3 and 5 for the data to plot towards the margin of the predicted pdf. As expected, no such trend is visually seen in the companion synthetic data plots shown for reference in Figs 3 and 5. Running the same tests on the corresponding 1-D uniformized data $\{t_i\}$ leads to $M_N = 0.122$ and $I_N = 2.35$ with probabilities $P(M_N) = 0.14$ and $P(I_N) = 0.06$, within perfectly acceptable ranges.

The power of 2-D unifomization is that it now allows us to also test the angular distribution of the data, and more generally its 2-D distribution.

First consider testing the angular distribution as defined by the second set of uniformized data $\{s_i\}$. Such tests can be carried out with exactly the same tools, that is, the KS and AD tests. However, precisely because the uniformized variable s can be seen as a renormalized angle (recall Fig. 5), one additional test turns out to be even more useful. This test, due to Kuiper (1960), also measures the way the empirical cdf $F_N(x)$ differs from the expected theoretical cfd $F(x) = x$, but in yet another way, particularly appropriate for testing variables on a circle:

(iii) the Kuiper-test uses the sum $V_N = D_+ + D_-$ of the two maxima $D_+ = \max(F_N(x) - x)$ and $D_- = \max(x - F_N(x))$ over [0, 1], and is therefore insensitive to the change of the starting point (as can easily be checked, D_+ and D_- change individually, but their sum V_N remains constant).

To apply this test, one just needs to compute the value of V_N from the data set $\{x_i\}$, $i = 1, \ldots N$ to be tested, and infer (from known software, e.g. Press *et al.* 2007) the probabilities $P(V_N)$ for the null hypothesis to have produced such large, or even larger, values for V_N.

Fig. 6(a) shows the cdf built from the uniformized data $\{s_i\}$ to be tested. Also shown is the cdf built from the companion synthetic data shown for reference in Figs 3 and 5. Building these cdfs amounts to count the number of data found as one rotates anticlockwise in the plots shown in Fig. 5. Not surprisingly, Fig. 6(a) again testifies for the contrast between the deficit of data West of the Down/North plane and the presence of a sector with a strong concentration of data East of this plan, as seen in Figs 3(a) and 5(a). As expected, far less contrast is to be found in the cdf of the companion synthetic data (Fig. 6 b). Applying the KS, AD and Kuiper tests to these cdfs confirms the statistical significance of these impressions. For the real uniformized data $\{s_i\}$ from the combined sites 17 and 18 ($N = 88$ data), this now leads to $M_N = 0.156$, $I_N = 2.62$ and $V_N = 0.240$ with probabilities $P(M_N) = 0.02$, $P(I_N) = 0.04$ and $P(V_N) = 0.0012$. Both the KS and AD tests thus already consider the combined data of sites 17 and 18 to be incompatible with the QC model at the 98 per cent and 96 per cent levels of confidence. The Kuiper test, however, is clearly the most stringent of all tests, confirming this at the very high 99.88 per cent level of confidence. This sharply contrasts with the results of the same tests applied to the synthetic data, which lead to $M_N = 0.085$, $I_N = 0.87$ and $V_N = 0.12$ with probabilities $P(M_N) = 0.52$, $P(I_N) = 0.43$ and $P(V_N) = 0.66$, all within reasonable ranges.

Simultaneously testing the two dimensions of the data distribution in the [0, 1] × [0, 1] unit square can also be done thanks to a 2-D generalization of the KS test (Fasano & Franceschini

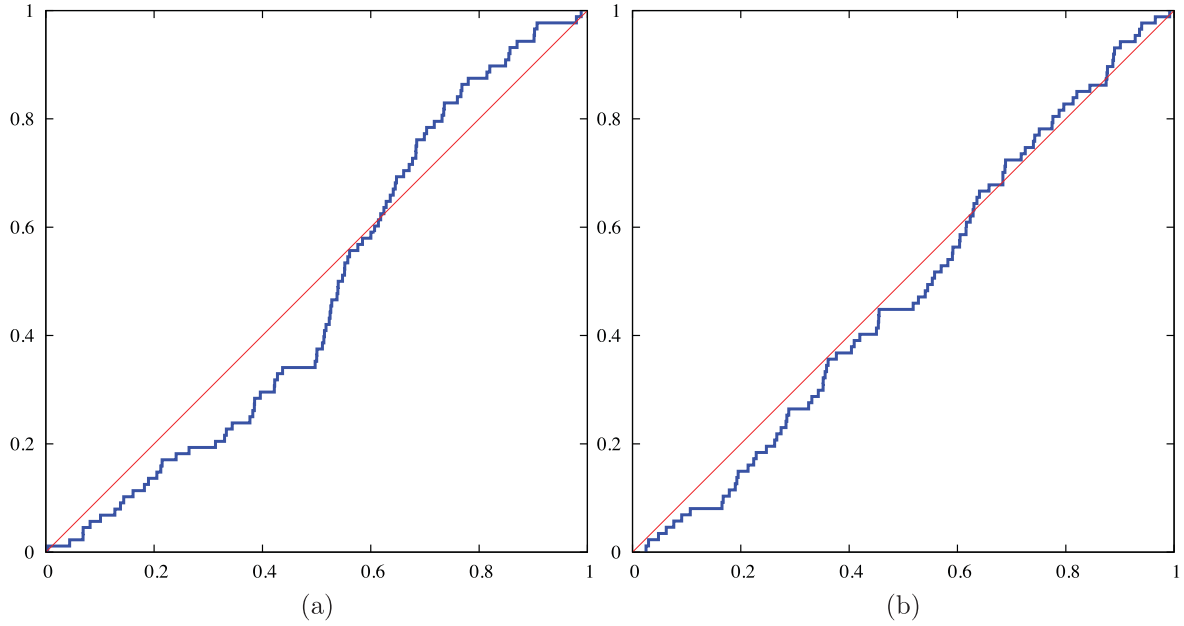

Figure 6. Empirical cumulative distribution function of the uniformized data $\{s_i\}$ corresponding to the combined data from sites 17 and 18 (shown in Fig. 3) tested against the QC model. (a) Real data; (b) synthetic data.

1987). This test, to which we will refer here as the FF test, is less straight-forward than the 1-D KS test. Unfortunately, it is also based on an empirical and approximate approach, since, as pointed out by Press *et al.* (2007, to which the reader is referred for more details) no universal cumulative probability distribution can be properly defined in more than one dimension. Nevertheless, this test can provide useful insight. When considering N data distributed in the unit square: the FF-test consists in (1) computing the empirical linear correlation coefficient r (Pearson's r) between the t and s coordinates, (2) defining a point Q of coordinates (t_Q, s_Q), (3) using Q to divide the unit square in quadrants (Q being their common edge), (4) comparing the empirical integrated probability (i.e. fraction of data found) in each quadrant with that expected from a uniform distribution and (5) identifying the quadrant with the largest difference (denoted D_N) between the empirical and expected integrated probabilities, when Q explores all locations in the unit square. The probability of finding such a discrepancy can then be assessed, and is here denoted $P(D_N, r)$.

This test was applied to the uniformized data of sites 17 and 18, and this led to $P(D_N, r) = 0.10$ corresponding to ($t_Q = 0.982$, $s_Q = 0.525$) because of the lower left quadrant being slightly underpopulated (see Fig. 4 a). The same test was applied to the synthetic data in Fig. 4(b) and led to $P(D_N, r) = 0.09$, now corresponding to ($t_Q = 0.466$, $s_Q = 0.224$) because of the upper left quadrant being slightly overpopulated. This result is interesting in several ways. It first shows that data from sites 17 and 18 cannot be considered as incompatible with the QC model based on this FF test alone, even though the test did spot an issue related to the cluster close to $t = 1$ and $s = 0.5$ we already mentioned. This cluster is detected as the cause of the lower left quadrant being slightly underpopulated, but not identified as unusually tight, even though this tightness clearly makes the distribution in Fig. 4(a) much more unusual than that in Fig. 4(b) (rightfully measured as not remarkably unusual). This is because the FF test restricts attention to the data distribution in four quadrants that may vary in size (depending on the location of Q), but must always share a corner with the unit square. This test is thus unable to spot the unusualness of a tight cluster away from any of the four corners of the unit square. This simply illustrates the well-known fact that no statistical test can singlehandedly test a given data set against a statistical distribution. In the present instance, we are thus led to conclude that the best test to detect the angular biases we are interested in is the Kuiper test applied to the $\{s_i\}$ uniformized data (see Table 1, which provides a summary of all tests carried out with the 2-D uniformized data of sites 17 and 18).

In closing this discussion about sites 17 and 18, it should finally be stressed that none of the above tests can tell which, of the data or the model (or both), should be rejected. As a matter of fact, data from sites 17 and 18 are likely to have serial correlations that could be responsible for the cluster discussed (see Khokhlov *et al.* 2006, for a detailed discussion). The important point, though, is that provided an appropriate test is being used, 2-D uniformization clearly makes it possible to spot mismatches between the data and the distribution predicted by a GGP model and the Fisherian errors assumed to affect these data.

We now turn to our second and final example application of the 2-D uniformization procedure to palaeomagnetic data. As already noted, one advantage of this procedure is that it makes it possible to collectively test the statistical behaviour of a large data set, even though each data may be expected to locally behave differently. This is exactly the case when one wants to test GGP models against a database with palaeomagnetic directional data coming from different sites worldwide.

To illustrate this situation, we generalize the tests carried out with the combined data of sites 17 and 18, to test all Brunhes data available in the Q94 database against the same QC model. This database, with 990 Brunhes data coming from 36 sites all over the world, was already investigated by Khokhlov *et al.* (2006), to test a series of GGP models. They already relied on the 1-D uniformized data $\{t_i\}$ as defined by (12), and tested the expected uniform distribution of these $\{t_i\}$ in the unit segment [0, 1]. Using the AD and KS tests then led them to reject all GGP models, except the QC model. This model, however, involves symmetries that cannot account for data trends such as the right-handed effect (Wilson 1970, 1972), which corresponds to a slight trend towards positive declination in the directional data, that is, towards East when the data are plotted in the same way as in Fig. 3, where this effect is particularly obvious. Quidelleur *et al.* (1994) noted that this effect collectively affects most normal data in their database (see their fig. 4). To test if this effect (whether linked to a bias in the data or not) is strong enough that the QC model should also be rejected can now easily be done by also taking advantage of 2-D uniformization.

Fig. 7(a) shows a plot of the 990 2-D uniformized data $\{(t_1, s_1), (t_2, s_2), \dots\}$ (each data having been assigned its individual error), computed from the Brunhes data of the Q94 database, using the QC model. These data are plotted in the disc of unit radius as in Fig. 5(a), and could have also been plotted in the unit square as in Fig. 4(a). Note, however, that no single plot analogous to Fig. 3 can now be shown, since such plots depend on the location of the site from which the data come. Just as in Fig. 5, Fig. 7(b) also shows a plot of the same amount (990) of 2-D uniformized data, corresponding to a set of 990 synthetic data produced from the QC GGP model, one datum at a time with $\mathfrak{p}_i(\mathbf{u})$ adjusted at each draw to exactly match the site location and assumed error of one true datum for each datum generated. Just like Fig. 5(b), this plot illustrates how the same number of synthetic data, intrinsically compatible with the QC model, with the same site distribution, and affected by the same individual errors as the true data, generally plot.

It is clear from Fig. 7 that if a right-handed effect is affecting the real data in a way incompatible with the QC model, this effect, which would translate in more data on average in the right half disc of the plot in Fig. 7(a) (as was the case in Fig. 5a) remains weak: Figs 7(a) and (b) could easily be confused with each other. However, the eye can easily be misled. Indeed, if one now plots the cdf built from the angular uniformized data $\{s_i\}$ (Fig. 8), a clearer picture emerges, with a slight overrepresentation of s values

Table 1. Results of the AD, KS, Kuiper and FF tests applied to the uniformized $\{(t_i, s_i)\}$ combined real data from sites 17 and 18 of Q94 and to synthetic data, for testing against the QC model. Probabilities of less than 0.05 are highlighted in bold.

Data [N]	$P(M_N[t])$	$P(I_N[t])$	$P(M_N[s])$	$P(I_N[s])$	$P(V_N[s])$	$P(D_N, r)$
Real [88]	0.16	**0.02**	**0.02**	**0.04**	**0.0012**	0.1
Synt [88]	0.14	0.06	0.52	0.43	0.66	0.07

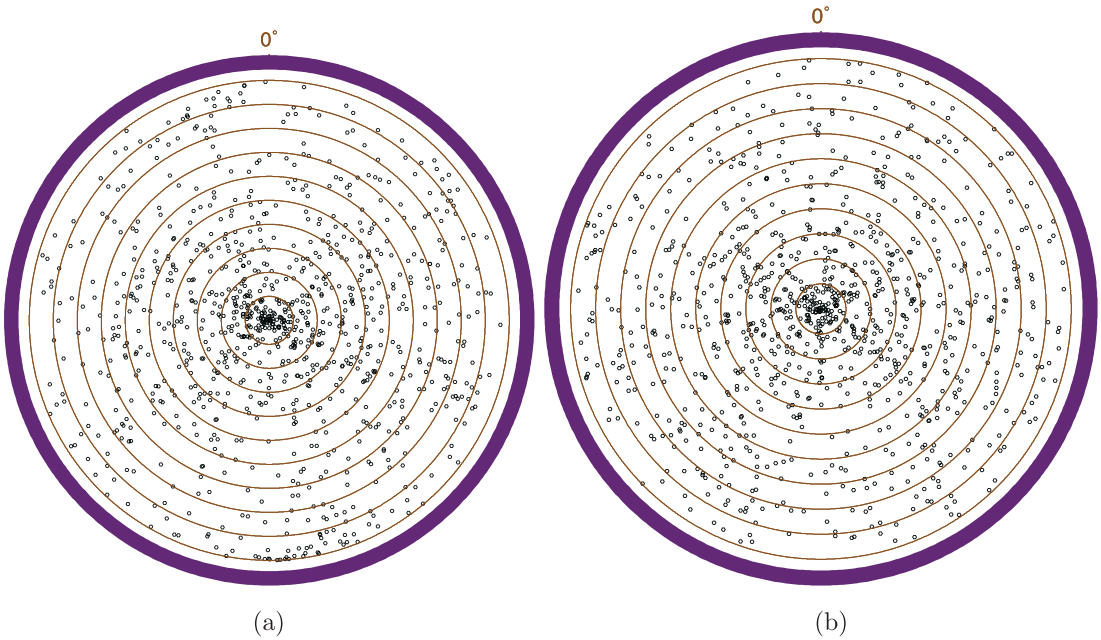

Figure 7. (a) 2-D uniformized data computed from the 990 Brunhes data of the Q94 database, using the QC model, plotted in polar $(t, 2\pi s)$ coordinates in a disc of unit radius; (b) same, but for synthetic data (see text for details). Same plotting convention as in Fig. 5.

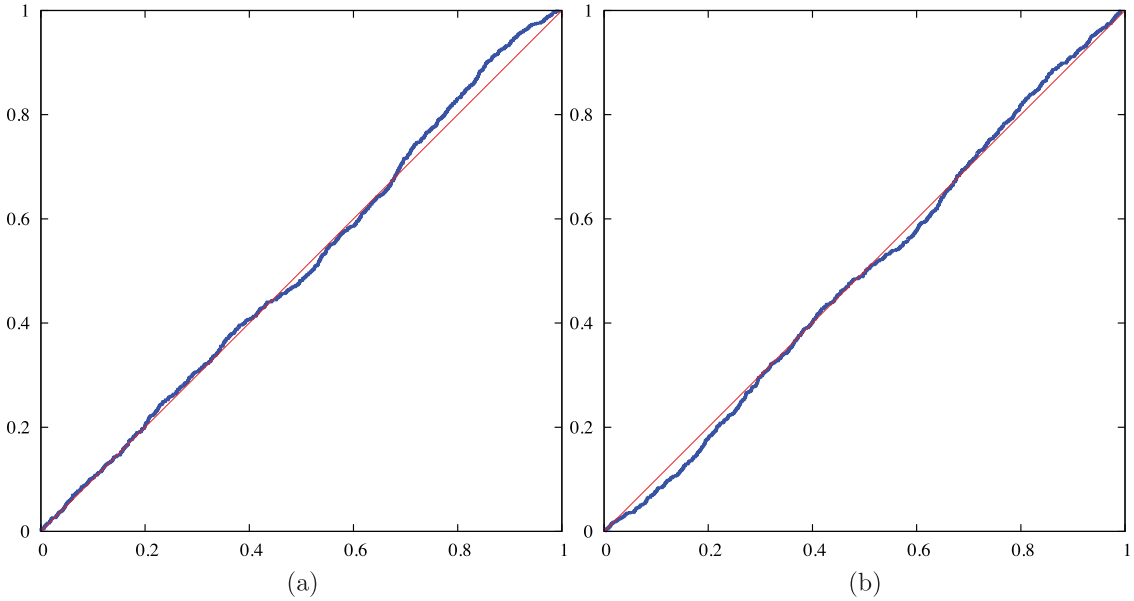

Figure 8. Empirical cumulative distribution function of the uniformized data $\{s_i\}$ corresponding to the 990 Brunhes data of the Q94 database tested against the QC model. (a) Real data; (b) synthetic data.

between 0.7 and 0.9 in Fig. 8(a). This overrepresentation turns out to be statistically significant.

Just as in the case of our previous investigation of the data from sites 17 and 18, we can again apply the KS, AD and Kuiper tests to the cdfs of both the $\{t_i\}$ and $\{s_i\}$ uniformized data, and the FF to the entire 2-D distribution. As already stated, the case of the $\{t_i\}$ data was already investigated by Khokhlov *et al.* (2006), and the corresponding cdf found to show no significant departure from the expected behaviour. We repeated these tests with our new, more accurate, numerical scheme to compute the convolution involved in (11). This led to the same conclusion (see Table 2) that the QC model could not be considered incompatible with these Brunhes data, based on the $\{t_i\}$ uniformized data alone. 2-D uniformization, however, provides critical additional information, in particular the second uniformized data $\{s_i\}$. Although the KS, AD and even the FF tests do not reveal more reasons to reject the tested hypothesis, the Kuiper test does, at the already strong level of 99 per cent (see Table 2). As expected, no such strong conclusion is reached when testing the 990 synthetic data plotted in Figs 7(b) and 8(b) (see also Table 2).

4 CONCLUSION

In this paper, following an approach similar to that of Rosenblatt (1952), we introduced the concept of 2-D probability uniformization, which allows the conversion of any 2-D probability distribution

Table 2. Results of the AD, KS, Kuiper and FF tests applied to the uniformized $\{(t_i, s_i)\}$ data from the 990 Brunhes data of the Q94 database and to synthetic data, for testing against the QC model. Probabilities of less than 0.05 are highlighted in bold.

Data [N]	$P(M_N[t])$	$P(I_N[t])$	$P(M_N[s])$	$P(I_N[s])$	$P(V_N[s])$	$P(D_N, r)$
Real [990]	0.30	0.26	0.10	0.07	**0.01**	0.07
Synt [990]	0.80	0.71	0.21	0.11	0.17	0.20

into an equivalent uniform distribution in the unit square $[0, 1] \times [0, 1]$. This concept is particularly useful for the purpose of testing data sets that have to be tested against different expressions of a common background statistics. This situation is typically encountered when testing so-called GGP models of the Earth's magnetic field against palaeomagnetic directional data collected from different geographical sites. We explained the way this approach could be applied to the 2-D distributions expected for such palaeomagnetic directional data, if these are to be consistent with a GGP model while affected by some Fisherian error.

We provided some example applications to real palaeomagnetic data. In particular, we showed how the significance of subtle inhomogeneities in the distribution of the data, such as the so-called right-handed effect in palaeomagnetism, could be tested. This effect, whether of geomagnetic origin or not, was already known to affect the Brunhes data, particularly that of the Quidelleur *et al.* (1994) database. Our probability uniformization approach allowed us to show that this right-handed effect indeed affects these data in such a way that they cannot easily be reconciled with the QC model [the preferred model C1 of Quidelleur & Courtillot (1996), which is rejected at the 99 per cent level of confidence, recall Table 2], even though this model was originally built with the help of these data. This approach was also applied at the level of single sites [sites 17 and 18 of the Quidelleur *et al.* (1994) database] to confirm that data that one could intuitively see as affected by the same effect (this time in a strong way, recall Fig. 3), also could not be reconciled with this same model (this time at a much higher level of confidence, recall Table 1).

These results show that 2-D probability uniformization could be systematically used to both test data at the site level (to possibly identify issues with the data themselves), and test GGP models of the mean palaeomagnetic field and palaeosecular variation against well-controlled palaeomagnetic data sets, such as those carefully put together within the context of the TAFI project (see e.g. Johnson *et al.* 2008), and archived in the Magnetic Information Consortium (MagIC) archiving system (http://earthref.org/MAGIC/). It is our hope, and opinion, that this procedure could help in building more accurate GGP models. The software designed in the course of this study is available upon request from the authors. It can also be downloaded from http://geomag.ipgp.fr/download/PSVT.tgz.

ACKNOWLEDGMENTS

The authors wish to thank the editor and two anonymous reviewers for their very useful comments, Petr Akhmetiev for his important critics of an early version of this paper, and J.-L. le Mouël for fruitful discussions and help. This work was partly supported by RFBR grant N11-05-00601. This is IPGP contribution N° 3357.

REFERENCES

Bingham, C., 1964. Distributions on sphere and on the projective plane, *PhD thesis,* Yale Univ., New Haven.

Bingham, C., 1983. A series expansion for angular Gaussian distribution, in *Statistics on Spheres,* pp. 226–231, ed. Watson, C., Wiley-Interscience.

Böhnel, H., Kohnen, H., Negendank, J. & Schmincke, H.-U., 1982. Palaeomagnetism of Quaternary volcanics of the East-Eifel, Germany, *J. Geophys.,* **51,** 29-37.

Böhnel, H., Reismann, N., Jäger, G., Haverkamp, U., Negendank, J.F.W. & Schmincke, H.-U., 1987. Paleomagnetic investigation of Quaternary West Eifel volcanics (Germany): indication for increased volcanic activity during geomagnetic excursion/event? *J. Geophys.,* **62,** 50–61.

Bouligand, C., Hulot, G., Khokhlov, A. & Glatzmaier, G.A., 2005. Statistical paleomagnetic field modelling and dynamo numerical simulation, *Geophys. J. Int.,* **161,** 603–626.

Constable, C.G. & Parker, R.L., 1998. Statistics of the geomagnetic secular variation for the past 5-My, *Geophys. J. Int.,* **93**(B10), 11 569–11 581.

Donadini, F., Korte, M. & Constable, C., 2010. Millennial variations of the geomagnetic field: from data recovery to field reconstruction, *Space Sci. Rev.,* **155,** 219–246.

Fasano, G. & Franceschini, A., 1987. A multidimensional version of the Kolomogorov-Smirnov test, *Mon. Not. R. astr. Soc.,* **225**(1), 155–170.

Fisher, R., 1953. Dispersion on a sphere, *Proc. R. Soc. Lond., A,* **217,** 295–305.

Fisher, N., Lewis, T. & Embleton, B., 1987. *Statistical Analysis of Spherical Data,* Cambridge University Press, Cambridge.

Healy, D., Jr, Rockmore, D., Kostelec, P.J. & Moore, S.S.B., 1996. FFTs for the 2-sphere: improvements and variations, *J. Fourier Anal. Appl.,* **9,** 341–385.

Hongre, L., Hulot, G. & Khokhlov, A., 1998. An analysis of the geomagnetic field over the past 2000 years, *Phys. Earth planet. Int.,* **106,** 311–335.

Hulot, G. & Le Mouël, J-L., 1994. A statistical approach to the Earth's main magnetic field, *Phys. Earth planet. Int.,* **82,** 167–183.

Hulot, G. & Bouligand, C., 2005. Statistical paleomagnetic field modelling and symmetry considerations, *Geophys. J. Int.,* **161,** 591–602.

Hulot, G., Finlay, C.C., Constable, C.G., Olsen, N. & Mandea, M., 2010. The magnetic field of planet Earth, *Space Sci. Rev.,* **152,** 159–222.

Jackson, A., Jonkers, A.R.T. & Walker, M.R., 2000. Four centuries of geomagnetic secular variation from historical records, *Phil. Trans. R. Soc. Lond., A.,* **358,** 957–990.

Johnson, C.L. *et al.*, 2008. Recent investigations of the 0-5 Ma geomagnetic field recorded by lava flows, *Geochem. Geophys. Geosyst.,* **9**(4), Q04032, doi:10.1029/2007GC001696.

Khokhlov, A., Hulot, G. & Carlut, J., 2001. Towards a self-consistent approach to palaeomagnetic field modelling, *Geophys. J. Int.,* **145**(1), 157–171.

Khokhlov, A., Hulot, G. & Bouligand, C., 2006. Testing statistical palaeomagnetic field models against directional data affected by measurement errors, *Geophys. J. Int.,* **167**(2), 635–648.

Kono, M. & Tanaka, H., 1995. Mapping the Gauss coefficients to the pole and the models of paleosecular variation, *J. Geomag. Geoelectr.,* **47,** 115–130.

Kuiper, N.H., 1960. Tests concerning random points on a circle, *Proceedings of the Koninklijke Nederlandse Akademie van Wetenschappen, A,* **63,** 38–47.

Lévy, P., 1937. *Théory de l'Addition des Variables Aléatoires,* Gauthier-Villars, Paris, pp. 71–73 and 121–123.

Lhuillier, F., Fournier, A., Hulot, G. & Aubert, J., 2011. The geomagnetic secular-variation timescale in observations and numerical dynamo models, *Geophys. Res. Lett.,* **38,** L09306, doi:10.1029/2011GL047356.

Love, J.J., 2007. Bingham statistics, in *Encyclopedia of Geomagnetism and Paleomagnetism,* eds Gubbins, D. & Herrero-Bervera, E., Springer, Heidelberg.

Love, J.J. & Constable, C.G., 2003. Gaussian statistics for palaeomagnetic vectors, *Geophys. J. Int.,* **152**(3), 515–565.

Marsaglia, G. & Marsaglia, J.C.W., 2004. Evaluating the Anderson-Darling distribution, *J. Statist. Soft.,* **9**(2), 1–5.

Matzka, J., Chulliat, A., Mandea, M., Finlay, C.C. & Qamili, E., 2010. Geomagnetic observations for main field studies: from ground to space, *Space Sci. Rev.,* **155,** 177–218.

O'Reilly, F.J. & Quesenberry, C.P., 1973. The conditional probability integral transformation and applications to obtain composite Chi-square goodness-of-fit tests, *Ann. Statist.,* **1**(1), 74–83.

Olsen, N., Hulot, G. & Sabaka, T. J., 2010. Measuring the Earth's magnetic field from space: concepts of past, present and future missions, *Space Sci. Rev.,* **155,** 65–93.

Press, C., Teukolsky, S., Vetterling, W. & Flannery, B., 2007. *Numerical Recipes in C++,* 3rd edn. Available at: http://www.nr.com [accessed on 12 January 2013].

Quidelleur, X. & Courtillot, V., 1996. On low-degree spherical harmonic models of paleosecular variation, *Phys. Earth planet. Inter.,* **95**(1–2), 55–77.

Quidelleur, X., Valet, J.-P., Courtillot, V. & Hulot, G., 1994. Long-term geometry of the geomagnetic field for the last five million years: an updated secular variation database, *Geophys. Res. Lett.,* **21,** 1639–1642.

Rosenblatt, M., 1952. Remarks on a multivariate transformation, *Ann. Math. Statist.,* **23**(3), 470–472.

Tauxe, L., 2009. *Essentials of paleomagnetism*. Available at: http://magician.ucsd.edu/essentials/WebBook.html [accessed on 12 January 2013].

Tauxe, L. & Kent, D.V., 2004. A simplified statistical model for the the geomagnetic field and the detection of shallow bias in paleomagnetic inclinations: was the ancient magnetic field dipolar? in *Timescales of the Paleomagnetic field,* Vol. 145, pp. 101–115, eds Channell, J.E.T., Kent, D.V., Lowrie, W. & Meert, J., Am. Geophys. Un. Monongr.

Wilson, R.L., 1970. Permanent aspects of the Earth's non-dipole magnetic field over upper Tertiary times, *Geophys. J. R. astr. Soc.,* **19,** 417–437.

Wilson, R.L., 1971. Dipole offset-the time-averaged paleomagnetic field over the past 25 million years, *Geophys. J. R. astr. Soc.,* **22,** 491–504.

Wilson, R.L., 1972. Paleomagnetic differences between normal and reversed field sources, and the problem of far-sided and right-handed pole positions, *Geophys. J. R. astr. Soc.,* **28,** 295–304.

APPENDIX

The exact choice of the spherical grid to be used is important for the uniformization procedure on the unit sphere S^2. Numerical integrations over spherical domains are needed twice: in (11) when convolving a Fisher distribution with the local Angular Gaussian distribution to compute the $\mathfrak{p}_i(\mathbf{u})$ pdf, and in (12) when computing t_i from $\mathfrak{p}_i$. Such integrations can be realized along the lines of Press *et al.* (2007). However, since we lack an explicit formula for $\mathfrak{p}_i(\mathbf{u})$, the computational cost is rapidly increasing with the number of gridpoints. A proper choice of grid, however, can significantly reduce this cost. The idea is to use an analogue of the known 'Convolution using Fast Fourier Transform' procedure appropriate for scalar functions of one variable (Press *et al.* 2007). Here we use the fast discrete Legendre transform and the fast discrete Fourier transform from Healy *et al.* (1996). The corresponding grid is fully determined by its 'bandwidth' parameter B: in usual θ, φ spherical coordinates, the $2B \times 2B$ gridpoints $\mathbf{u}_{k,j}$, $0 \leq k, j < 2B$ are

$$\mathbf{u}_{k,j} = \{\theta_k, \varphi_j\} = \left\{ \frac{\pi(2k+1)}{4B}, \frac{\pi j}{B} \right\}.$$

The construction of such a fast transform involves a lot of computer code, and we therefore rely (with only minor changes) on the S2Kit C-subroutines by Peter J.Kostelec and Daniel N. Rockmore available from http://www.cs.dartmouth.edu/~geelong/sphere/. For the statistical analysis presented in this paper, we tried several values of the bandwidth parameter B between 180 and 1440. The results presented in Tables 1 and 2 were computed with $B = 720$, which was found to be appropriate enough.